Deactivation, reactivation and super-activation of Fe-N/C oxygen reduction electrocatalysts: gas sorption, physical and electrochemical investigation using NO and O_2

Paul Boldrin[b], Daniel Malko[a], Asad Mehmood[a], Ulrike I. Kramm[c], Stephen Paul[c], , Stephan Wagner[c], Natascha Weidler[c], Anthony Kucernak[a,*]

[a] Department of Chemistry, Imperial College London, London UK

[b] Department of Earths Science and Engineering, Imperial College London, London UK

[c] FG Katalysatoren und Elektrokatalysatoren, Technische Universität Darmstadt, Darmstadt, Germany

Abstract

We show that gaseous nitric oxide(NO) and oxygen(O_2) are useful molecular probes for Fe-NC catalysts. We examine using gaseous NO in a temperature programmed desorption experiment with using it in an electrochemical experiment. Gas phase O_2 adsorption is almost exclusively desorbed as CO_2, and continued exposure to oxygen increases the amount of chemisorbed oxygen. The oxidation state of the carbon surface is an important activity determining factor, and under normal "electrochemical" conditions many of the active sites are blocked. Treatment at 600°C in Ar can free those sites for oxygen adsorption. However, under atmospheric storage, and especially during the oxygen reduction reaction (ORR), the surface quickly becomes deactivated with chemisorbed oxygen species and water. We demonstrate that Fe-NC can be super-activated by reductive electrochemical treatment, both in an electrochemical cell and in a fuel cell. The energy gained following the treatment is significantly larger than the energetic cost.

1. Introduction

The activation of oxygen is crucial for electrochemical energy conversion in fuel cells and for the catalysed oxidation of chemical compounds. The most active known catalysts for oxygen (electro)catalysis are platinum group metals and alloys[1, 2]. However, these materials come with a high cost and are easily poisoned[3]. Therefore, alternatives are desirable.

A group of non-precious metal catalysts based on carbon which is doped with nitrogen and iron or cobalt, consist of abundant elements and show promising activity with interesting poison tolerance [4-10]. These materials have been extensively investigated for the electrochemical oxygen reduction reaction and recently for heterogeneous catalysis, such as epoxidations, oxidations and hydrogenations as well[11-14].

However, the activity of these materials is still significantly lower than their precious metal counterparts[15]. A better understanding of the underlying mechanisms which are responsible for the catalytic activity might enable improvement of these materials and allow other applications such as the activation of other small molecules.

The current consensus in the literature is that the metal species are present in the material as atomic active sites, embedded in the carbon matrix through coordination with 2 to 4 nitrogen atoms, which are present as pyridinic or pyrrolic nitrogen in the carbon lattice[8]. Although several high-quality publications offer insight into the physicochemical properties of these materials and important structure-property relationships have been established, the exact source and underlying mechanisms of catalytic activity are still nebulous[16-18]. Previously, Malko et al. found that nitric oxide (NO) and nitrite (NO_2^-) can be used as electrochemical probes and the material can be poisoned and recovered via electrochemical nitrite stripping[3] (shown as the red dotted pathway in Figure 1).

Recently, Choi et al. showed that the work function seems to be correlated with the electrochemical activity, implying that not only the active site, but also the surrounding electronic environment are important factors in determining the activity[19]. Kneebone *et* al have also used NO as a gas phase probe molecule to study this class of catalysts using Mössbauer and nuclear resonance vibrational spectroscopy[20].

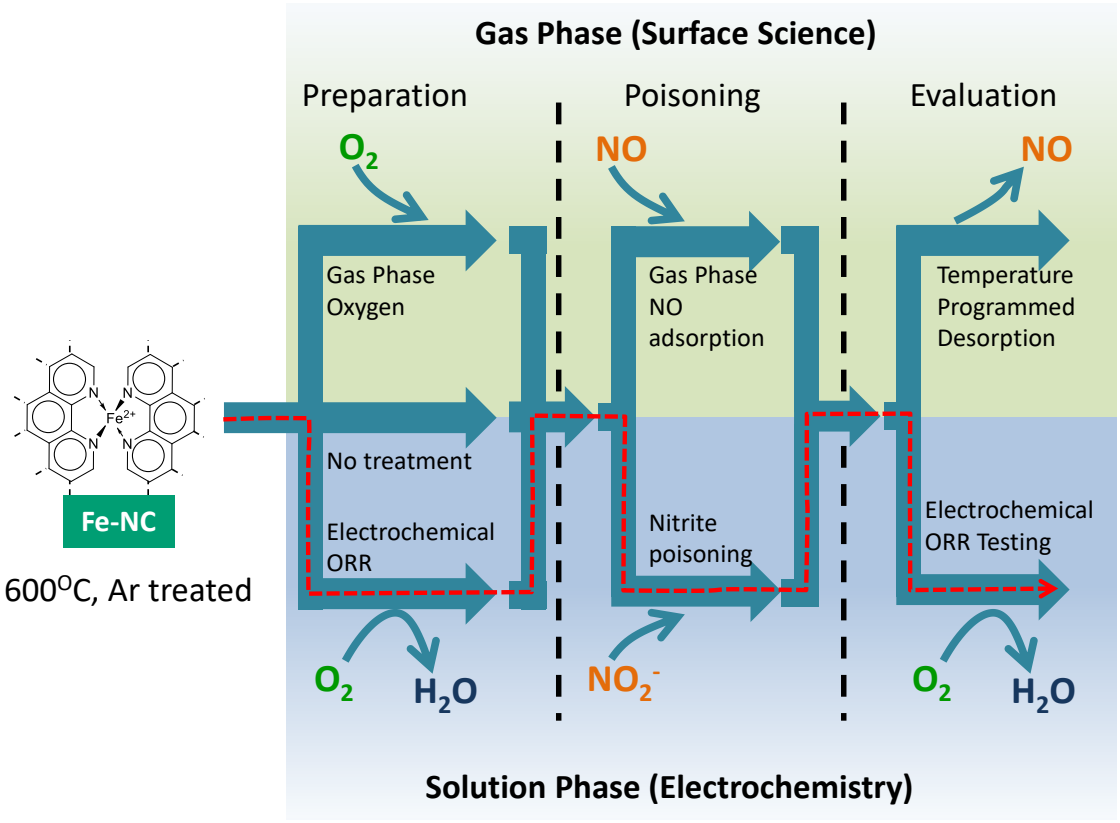

Figure 1 ¦ Experimental approach used in this paper. Combined electrochemical (lower half) and gas phase temperature programmed desorption (upper half) experiments associated with the quantification of Nitric oxide (NO, as a gas or as solution phase nitrite) blocking of sites responsible for oxygen reduction in acidic electrolytes. The red dotted path represents the Nitrite poisoning approach to quantify the number of active sites[3].

Here we show that NO can be used as a probe for Fe-N/C catalysts in chemisorption apparatus (top pathway in Figure 1) coupled to electrochemical and spectroscopic experiments (bottom pathway in figure 1). The Fe-NC catalyst used in this paper is the same as used in that paper and has already been extensively tested[3, 11, 21-25] and benchmarked against other Fe-NC catalysts[26]. It is shown via Mössbauer to consist virtually entirely of single atom D1 and D2 sites at an Fe loading of 1-1.5 wt%.[26] We examine this catalyst through three different sequential sets of experiments which can either take place in the gas phase or electrochemical phase. In all cases we start with a "cleaned" catalyst (600°C, Ar), Figure 1. In the first preparation phase, the catalyst is either exposed to (gas phase) oxygen or exposed to the electrochemical ORR environment, or used without any treatment (preparation phase, figure 1). In the poisoning phase, the catalyst is poisoned by either gas phase NO adsorption in a Temperature programmed desorption (TPD) apparatus or solution phase nitrite adsorption (poisoning phase, figure 1). Finally, we examine the electrochemical performance of the catalyst following the poisoning step and the amount of NO adsorbed in electrochemical or gas phase systems (Evaluation, Figure 1).

The combination of electrochemical and gas phase TPD experiments allow us to obtain a better understanding of the surface. In moving from the left hand side to right hand side of Figure 1 it will be

appreciated that there are 12 possible types of experiments and we examine almost all of them. We show that catalyst ORR activity is not only governed by the nature of the active site, but also by the state of the carbon surface surrounding the active site. Tracking gas adsorption and desorption of NO, O_2 and CO_2 on Fe-NC and correlating the results with XPS, Mössbauer and electrochemical activity we show that complex surface processes on the catalyst are important when considering the electrochemical activity towards oxygen reduction. Finally, we show that the catalyst can be super-activated via reductive treatment, and that this process is effective in an operational fuel cell. This implies that by modifying the carbon surface rather than the alleged iron active site it is possible to improve the catalytic activity. These rather unexpected results show that it is important not only to focus on the active site, which is believed to be the iron itself, but the overall catalytic system, when aiming to improve the activity of these materials.

2. Experimental

2.1 Catalyst Synthesis and properties: Fe-N/C (1.5±0.2 wt % iron determined via x-ray fluorescence) and nominally iron free, N/C (60±20 ppm iron via x-ray fluorescence) were prepared according to a previously reported method as described in supplementary section S1. Further details of the synthesis are described in [3, 23] and within which are complete characterisation details including XPS, TEM, HR-TEM, Lattice spacing analysis, X-Ray Fluorescence, and BET analysis. Note that this is the same catalyst which has undergone a benchmarking study against a number of other Fe-NC catalysts described in[26]. These catalysts have been extensively characterised and are composed of Fe-N_4 sites with no evidence of any carbide and minimal nitride phases in XRD, TEM microscopy[3, 26], and Mössbauer spectroscopy (minor contribution of nitride and sulfide phases, < 6.6 %, see below). For comparison, a high surface area carbon black with similar microporous surface area (Ketjen Black EC600-JD) was also tested (surface area measurements of all catalysts in Section S2).

2.2 Gas sorption analysis: All TPD experiments were carried out using a Micromeritics Autochem 2920 with an MKS Cirrus Mk2 mass spectrometer attached. All gases used are research grade (BOC industrial gases, UK). In all experiments, argon is used as the carrier gas, pure oxygen and 1% nitric oxide in argon are used to expose the samples to oxygen and nitric oxide respectively, while 1% CO_2 in argon, 2% O_2 in argon and 1% nitric oxide in argon are used to calibrate the mass spectrometer. The argon line runs through and oxygen and moisture traps (120cc Supelpure-O Oxygen/Moisture Trap, Sigma-Aldrich) to remove residual oxygen and water, while the oxygen and 1% nitric oxide lines run through moisture traps (200cc Supelpure Molecular Sieve 5A Moisture Trap). For experiments, approximately 20 mg of sample is placed on quartz wool in a quartz U-tube and the sample loaded into the equipment. Unless otherwise stated, all samples are first purged for at least 5 mins with argon before heating to 600 °C to clean the sample of adsorbed species. The sample is then exposed to the test gas (either 1% NO or oxygen) for 1 hour, before 1 hour of purging with argon. TPDs are then carried out using a ramp rate of 20 °C/min and a final dwell of 10 mins at the target temperature (600 °C except in the case of the cycling experiments, where 200 or 300 °C are used). After the completion of selected experiments the mass spectrometer was calibrated for nitric oxide, carbon dioxide and/or oxygen concentrations by flowing a selection of mixtures of the calibration gases with argon to create a calibration curve.

For NO TPDs, peak fitting was carried out in Origin, using a Gaussian fit for the high temperature peaks and a log normal fit for the low temperature peak. Activation energies and reaction orders were carried out according to the method of Parker, Jones and Koel[21] using the Gaussian fit of the high temperature peak. This involves plotting $\ln(-d\theta/dt)-n\ln(\theta)$ against $1/T$, where θ is the coverage, n is the reaction order and T is the temperature. For the correct value of n this gives a straight line in the region of the peak maximum, with a gradient of Ea/R where Ea is the activation energy and R is the

gas constant. Because the actual coverage is not known it was assumed that the coverage was 100% at t=0 and 0% at the end. This assumption makes no difference to the value calculated for the activation energy or the reaction order.

2.3 Surface Science analysis: X-ray photoelectron spectroscopy was performed under ultrahigh vacuum (UHV) on a hemispherical energy analyser PHOIBOS 150 from Specs™ Surface Nano Analysis GmbH, using an Al Kα X-ray source XR50M with an energy hν of 1486.6 eV and a line width of 0.85 eV. Electron detection was ensured by a CEM 9 Channeltron extended range channel electron multiplier detector from Specs™. Evaluation of the obtained spectra was performed using the program CasaXPS (Version 2.3.19PR1.0, Casa Software Ltd.), with all peaks referenced to literature assignments. Indium foil was used as substrate for the analysed catalyst powder. Peak fitting was done using a 30/70 mixed Gaussian/Lorentzian line shape and a Shirley background. Fine scan spectra were obtained from the regions for Fe 2p, N 1s, C 1s, O 1s and S 2p. The dwell time and energy step width for all fine scan spectra was 0.1 s and 0.05 eV, respectively, with a pass energy of 10 eV. For the N 1s and C 1s fine scan spectra 45 and 5 scans, respectively, were applied.

2.4 ^{57}Fe Mössbauer spectroscopy: ^{57}Fe Mössbauer spectroscopy was performed at room temperature in transmission mode using a scintillation detector for data acquisition and a ^{57}Co/Rh source to generate the relevant 14.4 keV gamma radiation. Measurements were made with triangular reference waveform with a 1024 multichannel analyser. The velocity axis is calibrated with respect to alpha iron (25 µm thickness, 99.99 % purity). For the assignment of iron species Lorentzian Site Analyses using the Recoil program were performed for the investigated catalysts.

2.5: Electrochemical analysis: For the electrochemical experiments using the Rotating Ring Disk Electrode (Pine Instruments, model AFE6R1AU having a mirror polished glassy carbon as disk and rotator model AFMSRCE), the catalyst was deposited on the glassy carbon disk following a procedure described in the literature. A three compartment electrochemical glass cell was used for the aqueous electrochemical tests, the electrolyte 0.5M H_2SO_4 was prepared by diluting 95% H_2SO_4 (Aristar, VWR) with ultrapure water (MilliQ 18.2 MΩ cm). The RHE reference electrode (self-made) was ionically connected to the main compartment of the electrochemical glass cell via a Luggin–Haber-capillary. A glassy carbon rod was used as counter electrode and ionically connected to the main compartment of the glass cell through a porous frit. Glassy carbon was used instead of Pt in order to avoid contamination with catalytically active precious metals. A potentiostat (Autolab, model PGSTAT20) was used for potential or current control during the electrochemical measurements. Ultrapure gases utilized were, nitrogen and oxygen (BIP plus-X47S, Air products). The nitrite adsorption and stripping analysis protocol is described in [3, 24] and were performed using 0.125 M $NaNO_3$ in pH 5.2 acetate buffer. Performing the nitrite stripping in slightly acidic environment aids the stripping process and contributes to more complete stripping. It is important to utilize a potentiostat with a current integrator (or analog linear scan generator) when performing the stripping measurements as normal staircase voltammetry will not correctly measure the charges associated with these processes.

2.6 Single PEFC test: For tests in a single Polymer Electrolyte Fuel Cell (PEFC), the Membrane Electrode Assembly (MEA) was prepared as per a procedure described in the literature[44]. The anode was a Johnson Matthey Reformate Cathode Electrode with a loading of 0.4 mg_{Pt} cm^{-2} electrode (Alfa Aesar, UK). The high loading was chosen in order to avoid any kinetic limitation induced by the anodic reaction. The polymeric electrolyte was a Nafion™ 212 membrane (from Ion Power). For the cathode, the Fe-N/C catalyst was quantitatively deposited on a 5 cm^2 gas diffusion layer (Toray Carbon Paper, Baselayered, TGP-H-60 from Alfa Aesar) as per literature procedure[44]. Humidity, temperature and gas flow rate were controlled using a Scribner FC test station (850e). Potential and current control were

performed using a Gamry Reference 3000 potentiostat. Oxygen (BIP Plus, Air Products) flow rate was 550 mL min^{-1} and hydrogen (BIP Plus, Air Products) flow rate was 150 mL min^{-1} in order to avoid the possibility of oxidant or fuel starvation, while relative humidity was 100% for both gases and cell temperature was maintained at 80°C.

3. Results & Discussion

3.1. NO Chemisorption Experiments

It has been observed previously that Fe-N/C materials are stably poisoned by NO_2^-, NO and hydroxylamine (NH_2OH) in an electrochemical environment[3, 24] and this effect can be used to probe the number density and activity of active sites[3]. This approach has also been used to benchmark this catalyst against a sample of other Fe-NC catalysts[26] wherein all catalysts are extensively characterised. We were intrigued as to whether NO could be used as a **gas phase** probe to reveal information about the structure of the active site, the mechanism and thermodynamics of the poisoning and to count the number of active sites in this class of catalysts as well[20]. Although CO has been used previously to estimate the number of active sites for the oxygen reduction reaction (ORR)[17], to our knowledge NO had not been used as such a probe molecule **in chemisorption experiments**. Furthermore, the interaction of CO with this class of catalyst is much weaker than with the platinum catalysts which are typically used for the ORR. Hence although it is currently *hypothesised* that chemisorbed CO binds to the same site in the Fe-NC catalysts as is used to perform the ORR, it is not possible to test this hypothesis as CO cannot be used to poison the catalyst in an **electrochemical** environment. If NO could be shown to interact with these Fe-N/C catalysts in the gas phase, then this would give us a useful bridge to the performance of the catalysts poisoned by NO in an electrochemical environment and to ascertain if both gas-phase/electrochemical processes are probing the same site.

Because of the above-ambient temperature binding of the NO, we are more easily able to control experimental parameters such as heating rates, allowing a much wider range of desorption experiments providing information on the kinetics and thermodynamics of the desorption. Furthermore, in these experiments we utilised chemisorption instrumentation with a mass spectroscopy detector, so we could determine the chemical nature of the species desorbed from the surface rather than the thermal conductivity detector often used in the CO adsorption analysis[17].

Fe-N/C samples were pre-treated to 600 °C in Ar for 10 mins and cooled before being exposed to flowing 1% NO in Ar at STP for 1 h. Temperature programmed desorption (TPD) was then carried out on the NO-treated material, heating at 20 °C min^{-1} to 600 °C in flowing Ar, figure 2(a). It is interesting to note that the NO adsorption occurs at room temperature, whereas the gas phase CO adsorption on these catalysts only occurs at low temperature (193 K)[17]. For comparison, we also performed experiments on the Fe-N/C catalyst which had been dried but not heat-treated in Ar at 600°C ("Fe-N/C no-HT"). On heating, the NO desorbs and can be detected by mass spectrometry (figure 2a). We observed that for the Fe-N/C material there were two desorption peaks, a lower temperature peak with a temperature of ~94 °C, and a higher temperature peak with a temperature of ~149 °C which appears as a shoulder on the larger low temperature peak. Two peaks have also been observed during the TPD of CO adsorbed on similar catalysts (although in that case the absorption must be performed at 193K and the peaks desorb at much lower temperatures)[17, 27].

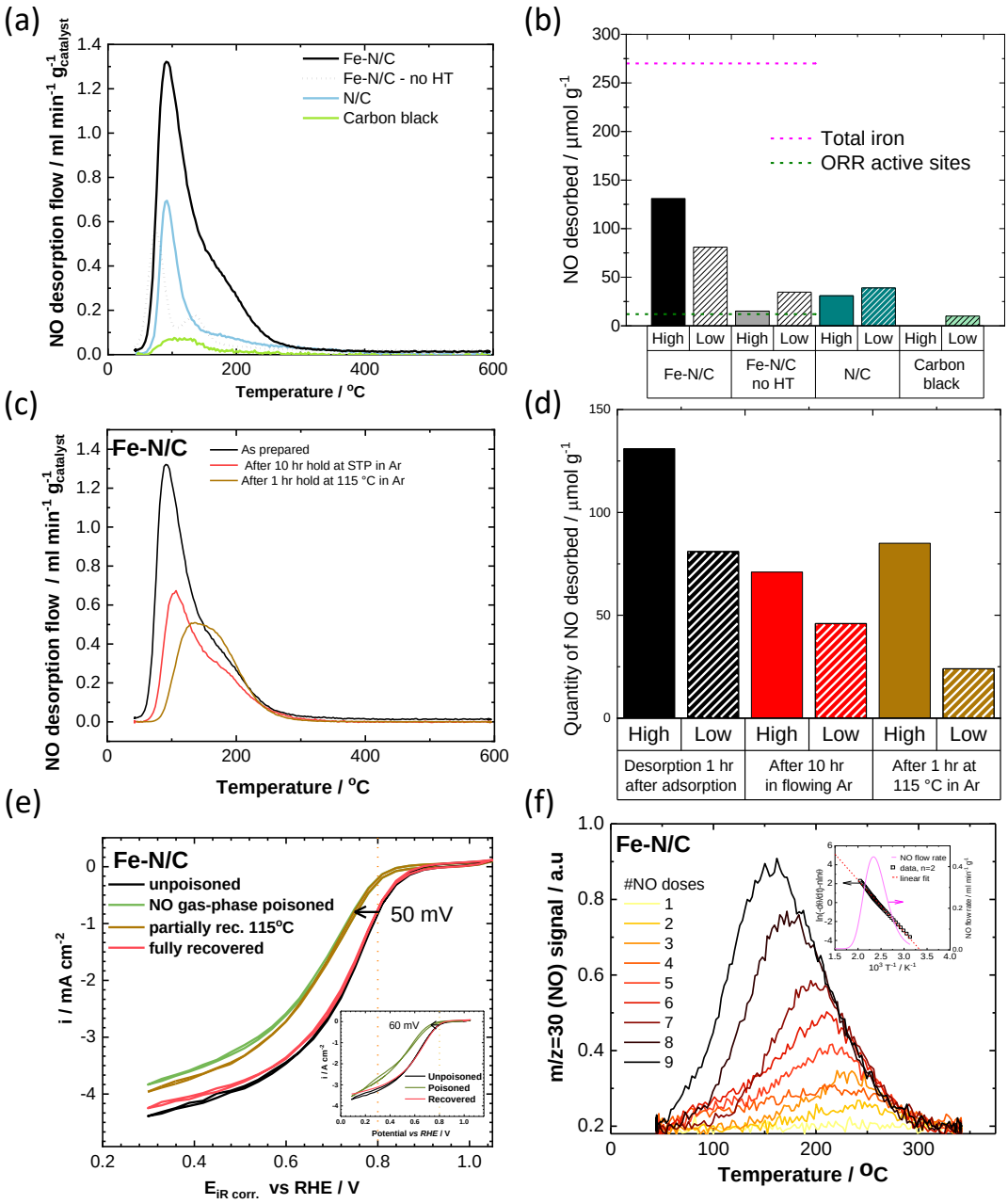

Figure 2 ¦ Gas phase NO poisoning and recovery of Fe-N/C catalysts. (a) Temperature programmed desorption curves for NO adsorbed onto Fe-N/C compared to N/C, and carbon black (Ketjen Black EC600-JD), all heat treated at 600 °C in Ar before NO adsorption except for "Fe-N/C-no HT", which was just dried. (b) Breakdown of the NO desorbed in (a) into high and low temperature components (bars), and for the Fe-N/C sample iron content and number of ORR sites (dashed lines) (see SI for details); (c) Temperature programmed desorption curves for NO adsorbed onto Fe-N/C, Fe-N/C exposed to 1% NO then flowing Ar for 10 hours at 40 °C and Fe-N/C exposed to 1% NO then held at 115 °C for 1 hour under flowing Ar. (d) Breakdown of the NO adsorbed in the peaks in (c) into high and low temperature components; (e) Electrochemical oxygen reduction curves for 600 °C cleaned Fe-N/C catalyst (unpoisoned) and the same catalyst treated with 1% NO in the gas phase for 1 hour (poisoned). This latter catalyst was also subjected to heat treatment at 600 °C to regenerate the initial activity (fully recovered). For comparison, the electrochemical ORR performance of a poisoned catalyst which has been heat treated at 115 °C for 1 hour in flowing argon is also shown (partially recovered). Inset: ORR curves for the same catalyst poisoned by solution phase NO. Electrochemical results performed in 0.5 M H_2SO_4, 1600 rpm, 5 mV s^{-1}, loading: 0.26 mg cm^{-2}. Solution phase NO poisoning performed by immersion of RDE electrode in a saturated nitric oxide/0.5 M Phosphate buffer solution at pH 7. (f) NO TPD for Fe-N/C samples exposed to increasing number of pulses of NO (1 pulse = 0.3793 mL of 1% NO). Inset: Graph of the fitted high temperature NO TPD peak for Fe-N/C exposed to 1% NO for 1 hour (black line) and the curve of ln(-dθ/dt)-nlnθ against 1/T for n=2 (black squares) and associated linear fit (dotted red line).

Figure 2(b) is a bar graph showing the amount of NO adsorbed on each type of site for each of the different catalysts in figure 2(a) (see S3 for details of peak deconvolution procedure). On the Fe-N/C catalyst, the amount of NO adsorbed in total was 212 $\mu mol_{NO}\ g_{Fe\text{-}N/C}^{-1}$, with 81 $\mu mol_{NO}\ g_{Fe\text{-}N/C}^{-1}$ on the low temperature peak and 131 $\mu mol_{NO}\ g_{Fe\text{-}N/C}^{-1}$ on the high temperature peak i.e. one NO molecule for every 4 nm^2 of total surface (see SI for BET data), or a separation of 1.3 nm between each NO molecule assuming hexagonal packing (if only the micropores are filled, this would corresponds to 3.3 nm^2 per NO and 1.1 nm separation). For context, the total amount of iron in the sample is 270 $\mu mol_{Fe}\ g_{Fe\text{-}N/C}^{-1}$ (dashed magenta line in the inset) - If all the iron is accessible and the NO only binds to those sites then 79% of the iron atoms would have NO bound to them. In contrast, our previous experimental work on this catalyst shows that the total number of sites active for the majority of the ORR current correspond to 12 $\mu mol\ g_{Fe\text{-}N/C}^{-1}$ [3](dashed olive line in the inset, i.e. equivalent to 4.4% of the iron in the sample). Hence much more NO is bound than can be explained on the basis of the electrochemically active sites.

NO gas phase adsorption was also carried out on a metal-free sample (N/C) prepared in the same way as the iron containing sample but without addition of any iron[3] and on a heat-treated carbon black (Ketjen Black EC600-JD). The amounts of NO adsorbed on these samples were far lower, only 70.1 $\mu mol_{NO}\ g_{N/C}^{-1}$ total NO adsorption in the case of the metal-free sample. This value is 3 times lower than that for the heat-treated Fe-N/C material, but very much larger than the total iron content in these "metal free" samples which contain less than 1 $\mu mol_{Fe}\ g_{N/C}^{-1}$. The metal-free sample also displays high and low temperature peaks, with 39.3 $\mu mol_{NO}\ g_{N/C}^{-1}$ on the low temperature peak and 30.8 $\mu mol_{NO}\ g_{N/C}^{-1}$ on the high temperature peak. These values are approximately two and four times less than the same values for the heat-treated Fe-N/C material. Note that the high temperature peak in the metal-free material is not very well fit using the same fitting parameters as in the Fe-N/C material, perhaps indicating that the mode of adsorption is different. For carbon black the amount of NO adsorbed was 10 $\mu mol_{NO}\ g_{carbon}^{-1}$, with only one, low temperature, peak present. This demonstrates that the sites which bind NO are far more prevalent in the Fe-N/C material than in the metal-free N/C material or the carbon black.

If we perform the NO TPD experiment on an Fe-N/C sample which has not been heated to 600°C before the NO adsorption ("Fe-N/C-no HT", dotted black line), we adsorb much less NO. Compared to the heat treated sample the low temperature peak shows a little under half as much NO adsorbed, whereas only about $1/10^{th}$ as much NO is adsorbed in the high temperature peak. It is interesting that the amount of NO adsorbed in the high temperature peak is 15 $\mu mol_{NO}\ g_{Fe\text{-}N/C}^{-1}$, similar to the value we obtain by NO adsorption and electrochemical stripping in an electrochemical cell[3]. We will return to this aspect below.

Removal of the majority of the NO associated with the low temperature peak may be accomplished by heating the NO-poisoned catalyst to 115 °C under flowing Ar for 1 h (figure 2c). TPD after this treatment showed that there was 120 $\mu mol_{NO}\ g_{Fe\text{-}N/C}^{-1}$ of NO remaining on the sample, with a peak maximum of 135 °C, indicating that the treatment had been successful in removing most of the low temperature NO. A similar effect to the heat treatment could also be accomplished by simply holding the catalyst at room temperature under flowing argon for 10 hours. See Figure 2(d) for a breakdown of NO distribution as a function of treatment regime for the response in figure 2(c).

In order to try and correlate NO gas-phase poisoning of the oxygen reduction sites of these materials, we also electrochemically tested the heat-treated and gas phase NO treated catalyst for activity towards the ORR using the rotating disk electrode approach, figure 2(e) (details in section S4). The degree to which the ORR is poisoned by the ex-situ NO gas phase treatment corresponds to a -50 mV shift in the ORR voltammogram, or about a 5 to 13-fold decrease in the kinetic current in the potential

range 0.80-0.85 V (section S5a), corresponding to an 80-92% reduction in ORR current. This is similar to the degree of poisoning achieved when an electrode composed of Fe-N/C is immersed in a NO-saturated phosphate buffer solution at pH 7 (ΔE = 60 mV, figure 2(e) inset)[24]. This shows that the gaseous phase NO treatment poisons the catalyst in a similar manner to liquid phase NO or liquid phase nitrite. Treating the gas phase NO treated Fe-NC at 115°C for one hour and performing the ORR measurement shows the same degree of poisoning. This suggests that it is the high temperature NO which results in catalyst poisoning. By comparison the N/C catalyst shows no deactivation when treated by either gas-phase or solution-phase NO [24](see section S5b). In contrast, if the sample is treated at 600 °C in Ar after poisoning with NO, then the activity is fully recovered to the same level as the original sample (figure 2e, fully recovered). This clearly suggests that it is the NO associated with the high temperature TPD peak which is responsible for the poisoning of the ORR, and that the low temperature NO is only present as a spectator species, as the catalyst shows a similar degree of poisoning in the absence of that NO.

However, there remains a conundrum. Our electrochemical stripping measurements on the same catalyst only shows 12 $\mu mol_{NO}\ g_{Fe\text{-}N/C}^{-1}$ of adsorbed NO[24], whereas the chemisorption results show an order of magnitude higher amount of strongly adsorbed NO (120 $\mu mol_{NO}\ g_{Fe\text{-}N/C}^{-1}$). Note that Malko et al found that at high nitrite concentration there was a non-specific adsorption of nitrite on the surface, and that this extra nitrite was relatively easily removed (see supplementary figure 20 and supplementary note 2 in reference [3]), suggesting a commonality between the gas phase and electrochemical experiments. Others too have seen an effect on the degree of poisoning with the amount of nitrite in solution[28]. Our conclusion is that under normal electrochemical/fuel cell conditions the majority of the NO adsorption sites (90% on the basis of the high temperature NO peak size in figure 2(a)) are blocked with adventitious adsorbates, the justification for which will be given below. Furthermore, the strongly adsorbing NO corresponding to the high temperature peak are adsorbed on sites which are responsible for the majority (80-92%) of the ORR in acid solution.

In order to better understand the nature of the NO adsorption on the samples, we performed pulse chemisorption experiments on the Fe-N/C catalysts used in figure 2(a). In these experiments we exposed the Fe-N/C samples to a fixed number of metered pulses of NO followed by TPD to study the energetics of the desorption process. The number and size of pulses were chosen to be in the domain where the sample is far away from saturation, and hence we do not see the low temperature NO desorption peak. The amount of NO desorbed is around a third of the total amount expected to be desorbed from the high temperature peak.

The change in peak position of the NO desorption and size with increasing amounts of NO on the surface is shown in figure 2(f). The peak maximum during NO desorption moves to lower temperatures and the high temperature edge of the peaks lines up for all levels of NO adsorption. Such a variation of peak shape with pulse number is qualitatively characteristic of a second order desorption process. Further information and confirmation of this assignment was achieved by performing analysis of the TPD measurements.

Deconvolution of the peaks to estimate the kinetic order of desorption[29] and activation energy was performed (see section S3 for details), giving a straight line for n=2, inset in Figure 2(f), again indicative of a second order desorption. The activation energy of the high temperature peak is found to be 46.1 kJ mol^{-1} which is indicative of a relatively weak chemisorption. These values are far below previously reported theoretical binding energies of NO to iron complexes of porphyrins and phthalocyanines (five-fold and six-fold coordinate iron), which range from 146 – 183 kJ mol^{-1} [30-32], while a study on

NO adsorption on initially four-fold coordinated ferrous Fe-N_4 (intermediate spin) substituted into graphene sheets found an even stronger binding energy of 211 kJ mol^{-1} [33].

Both the order of desorption of NO and the activation energy as measured by these TPD experiments are therefore inconsistent with a model which has NO binding to Fe sites similar to Fe-N_4 sites such as those in porphyrins. These would exhibit a first order desorption (since the only process occurring is the severing of a single NO bond to an Fe site) and as described above the activation energy for this would be expected to be much higher. Therefore, a new model for the binding of NO is required.

Previous work examining NO gas-phase adsorption on carbon has documented a second order desorption (n=2), and this has been ascribed to either the formation of NO dimers on the surface or that dimers are intermediates in the adsorption and desorption[34]. This causes a second order desorption to be observed as two processes are occurring – the severing of the NO dimer followed by the desorption of two NO molecules.

Interestingly, this behaviour has also been observed on activated carbon fibres, with more NO adsorbed by the fibres produced from PAN compared to those produced from cellulose or pitch[35]. This increased NO adsorption has been linked to nitrogen doping in other studies[36], while further studies demonstrated large increases in both the uptake and rate of uptake of NO upon impregnation of transition metal species such as iron and copper hydroxides[37, 38]. It has also been observed that NO adsorption on carbon is kinetically limited[39]. These observations are explained by a chemisorption-assisted spillover process[40], with NO filling micropores[41].

Measured heats of desorption are normally slightly lower than that measured here, for example 27 kJ mol^{-1} [38, 41] or 42 kJ mol^{-1} [34] but these are still in the weak chemisorption range as we measured. This interpretation of NO filling micropores is in reasonable agreement with literature regarding quantities of NO adsorbed[40, 41]. Our sample has a measured microporous volume of 0.123 cm^3 $g_{Fe\text{-}N/C}^{-1}$, with a total uptake of NO of 212 μmol_{NO} $g_{Fe\text{-}N/C}^{-1}$, while for example Alcañiz-Monge et al. measured a microporous volume of 0.13 cm^3/g with an NO uptake of 300 μmol_{NO} g_{carbon}^{-1} after one hour of exposure to 5% NO/He for an iron and nitrogen-doped carbon[40]. The volume of adsorption we measured (212 μmol_{NO} $g_{Fe\text{-}N/C}^{-1}$) is equivalent to 5% micropore filling relative to the density of liquid NO (1.06 g cm^{-2}). Alternatively, if we assume that the NO dimers are solely adsorbed on the surface of the micropores, we can calculate a surface area from the literature value of the size of the dimer molecule[42]. This gives a surface area of 12.4 m^2 $g_{Fe\text{-}N/C}^{-1}$, significantly less than the value of microporous surface area (421 m^2 $g_{Fe\text{-}N/C}^{-1}$, SI section S2).

3.2. **XPS and Mössbauer analysis**

The hypothesis that NO is binding to the carbon surface would then seem to be consistent with the TPD results as described above. In order to further investigate this hypothesis we used XPS which is able to measure the interaction of the NO with the surface of the sample, along with Mössbauer spectroscopy which is highly sensitive to the coordination environment of the iron[43].

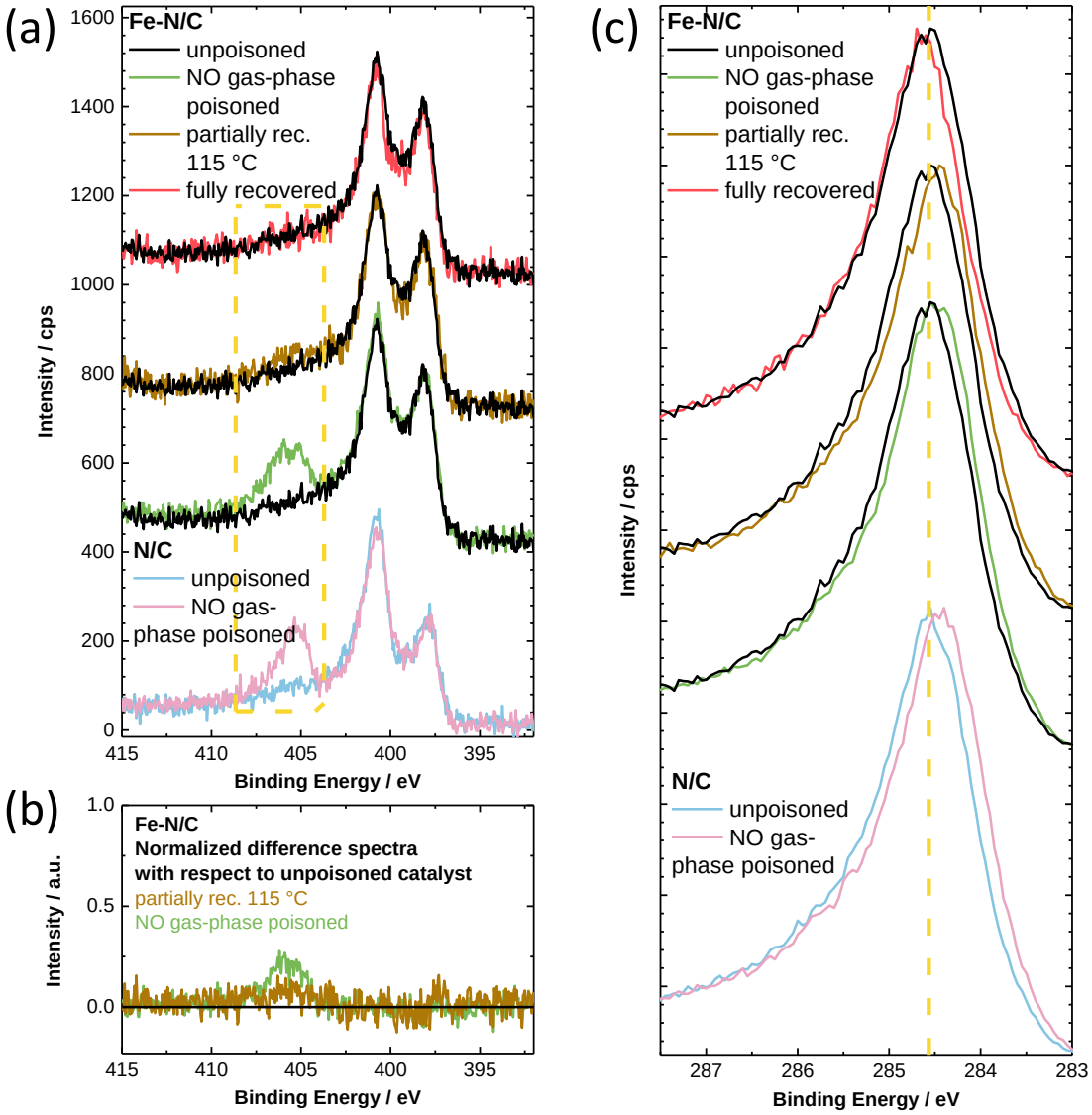

Figure 3 ¦ XPS of Fe-N/C and N/C catalysts as a function of poisoning. (a) Comparison of the N1s regions of the unpoisoned Fe-N/C with the NO gas-phase poisoned, partially recovered (115 °C) and fully recovered catalysts and for reasons of comparison N/C catalyst in unpoisoned and poisoned states. In (b) the difference spectra of the Fe-N/C catalysts in relation to the unpoisoned one are shown. (c) Comparison of the C1s regions of the unpoisoned Fe-N/C with the NO gas-phase poisoned, partially recovered (115 °C) and fully recovered catalysts and for reasons of comparison N/C catalyst in unpoisoned and poisoned state.

To get a better idea of how the NO interacts with the surface, X-ray photoelectron spectroscopy (XPS) was performed. The N1s regions of unpoisoned samples of both Fe-N/C and N/C (figure 3a) show two broad peaks at 398 and 401 eV, which encompasses the region in which peaks due to pyridinic, pyrrolic and graphitic nitrogen are found. In the samples exposed to gaseous NO in the same way described above, a broad peak appears between 404 and 408 eV that could be attributed to the formation of NO-interacting with FeN_4 sites (405 eV), NO_2 (405.2 eV) and NO_3 (407.5 eV)[44, 45] (see difference spectrum in figure 3b). However, in the sample of Fe-N/C which was heated to 115 °C after exposure to NO, this peak has largely disappeared, indicating that it is related to the low temperature NO desorption peak, which is not involved in the poisoning. In this sample, the region around 403 eV is more pronounced than in the unpoisoned sample. This would be consistent with the binding of the high temperature NO being as a dimer, since XPS peaks assigned to NO dimers have been seen in this

region in literature studies on NO adsorption on V, Ni and MoS_2[46, 47]. However, the N1s region is not conclusive to understand the interaction of NO with our Fe-N/C catalyst. Neither the poisoned or unpoisoned KB600 showed any response in the N1s region (see supplementary S6).

Another possible interaction is the direct adsorption of NO on the carbon. Indeed, the C1s spectra (normalized to 284.5 eV intensity, figure 3c) show that the poisoned samples reveal a shift towards lower binding energies, indicative of an increase in electron density on the carbon. This shift is found in the Fe-N/C exposed to NO and the sample heated to 115 °C after poisoning, and returns to its original position after heat treatment at 600 °C, suggesting that it must be associated with the high temperature NO. Interestingly the poisoned N/C sample also shows this shift whereas KB600 shows no shift on adsorption of NO (supplementary figure S5)

Mössbauer spectroscopy was also performed, and the spectra of all Fe-N/C catalysts are almost identical (see Supplementary Information, Table S2 for Mössbauer parameters and supplementary figure S7 for the individually fitted Mössbauer spectra) with < 6.6 % nitride and sulfide species. The remaining content is most possibly assigned to FeN_4 sites, only. Accordingly, 1.4 wt% Fe or ca. 250 µmol FeN_4 $g_{Fe\text{-}N/C}^{-1}$ are present in the catalyst. Assuming a homogeneous distribution over the overall surface area, this would correspond to 3.5 nm^2 per FeN_4-site (or 2.8 nm^2 per FeN_4 site if only the micropore surface area is considered). In the presence of NO the Mössbauer spectra are almost unchanged. If only the 12 µmol $g_{Fe\text{-}N/C}^{-1}$ measured by the electrochemical method is adsorbed directly on an FeN_4 site, a change of < 5 % of the Mössbauer spectrum would be expected. A test of simulating the spectra with 5 % of the absorption attributed to an FeN_4-NO interaction (see Kneebone et al. for the related Mössbauer parameters[20]) confirms that such change would be hard to see (not shown).

3.3. **Oxygen chemisorption and deactivation of the catalyst**

Because of the findings that the majority of NO is binding to carbon, we reason that the carbon must be in some way important for the ORR activity. We exposed the Fe-N/C to O_2 then performed TPD to examine the interactions of oxygen with the catalyst (figure 4a). TPD monitoring the concentrations of CO_2 and O_2 reveals that a small amount of oxygen (0.7%, or 1.4 μmol_{O2} $g_{Fe\text{-}N/C}^{-1}$) is reversibly adsorbed but the bulk is desorbed as CO_2. In total, 195 μmol_{O2} $g_{Fe\text{-}N/C}^{-1}$ of oxygen is desorbed either as CO_2 or O_2 which can be compared to a total of 270 μmol_{Fe} $g_{Fe\text{-}N/C}^{-1}$ of iron. While this is strikingly similar to the value of 212 μmol_{NO} $g_{Fe\text{-}N/C}^{-1}$ for NO adsorption, the species are adsorbing on different sites as the quantity of NO adsorbed is not reduced by pre-adsorption of O_2 and vice versa (see supplementary information section S8 for more details).

The reversibly adsorbed O_2 desorbs at around 70 °C, like NO desorption, a temperature which is characteristic of micropore filling. A supercritical gas would not desorb at such elevated temperatures in the absence of micropores or other specific binding sites[48]. CO_2 desorption occurs in two steps. There is a particularly low temperature desorption of CO_2 at ~90 °C with a well-defined peak followed by much broader emissions (centred around 200 °C) until around 500 °C where the CO_2 emissions begin to increase rapidly. Low temperature emission of CO_2 after exposure to oxygen has been previously observed on graphene and attributed to hydroxyl and epoxide groups[49, 50].

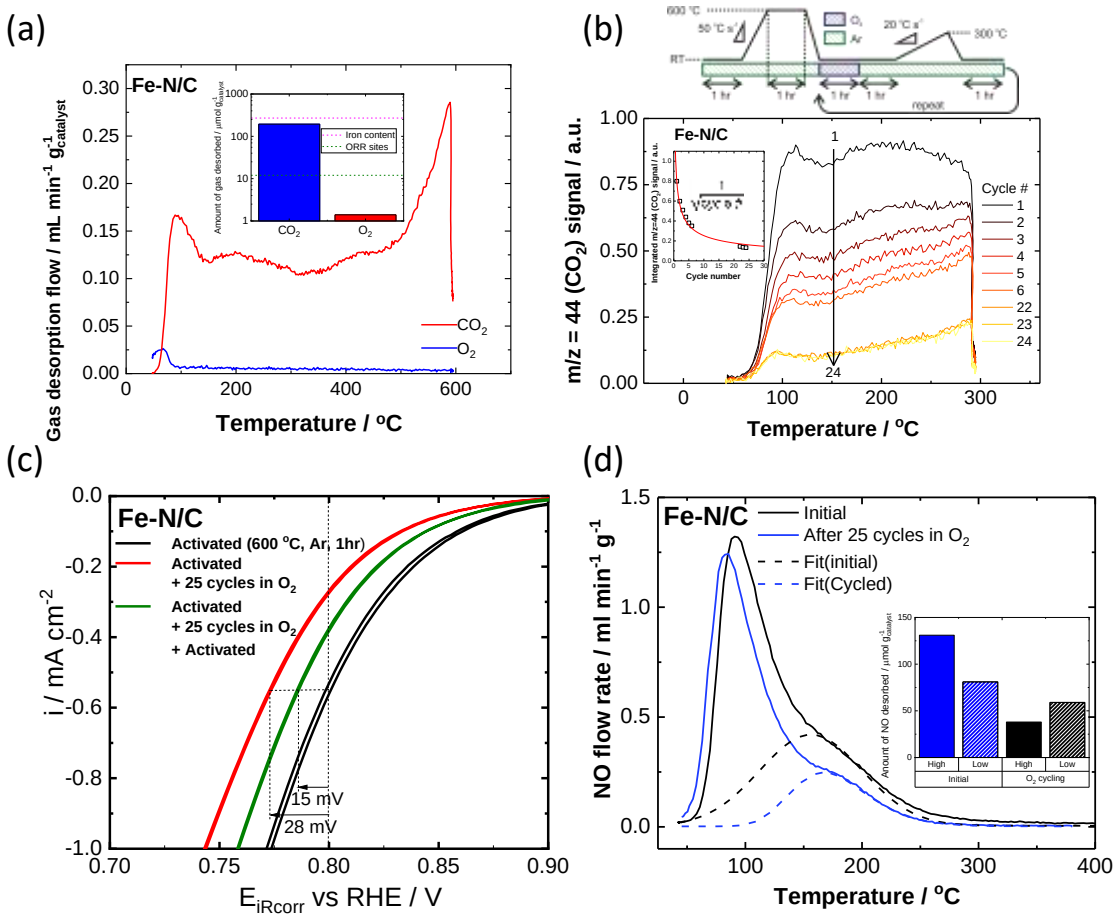

Figure 4 ¦ Quantification and effect of oxygenated species on electrochemical ORR performance and NO adsorption capacity of Fe-N/C catalysts. (a) Amount of CO_2 (red) and O_2 (blue) desorbed from Fe-N/C after exposure to O_2 for 1 hour at room temperature (b) Experimental design of the oxygen cycling experiments (top), consisting 25 cycles of 1 hour exposure to O_2 followed by a heat treatment to 300 °C under Ar and CO_2 desorption during the cycling (bottom), with the inset showing the total amount of CO_2 desorbed during each cycle, which decays exponentially with cycle number (c) RDE measurement of the as prepared Fe-N/C catalyst compared to a catalyst which was subjected to repeated heat treatment between room temperature and 300 °C for 25 times under oxygen atmosphere. Electrochemical results performed in 0.5 M H_2SO_4, 1600 rpm, 5 mV s^{-1}, loading: 0.26 mg cm^{-2}, (d) NO TPD before and after the oxygen cycling experiments between room temperature and 300 °C showing the large decreases in the high temperature NO peak (dotted lines) after cycling.

The carbon sites which adsorb oxygen then desorb CO_2 at 90 °C seem likely a prime candidate for being important for ORR activity. Oxygen adsorbing then desorbing as CO_2 must necessarily be destructive. Hence we decided to see if we could remove all these sites, and what the effect on activity would be. The Fe-N/C material was exposed to oxygen for one hour, then a temperature ramp imposed (20 °C min^{-1}) in argon up to a maximum temperature of either 200 °C or 300 °C. The sample was then cooled to RT under argon and re-exposed to oxygen for one hour. This was repeated 23 times (figure 4b). The TPD shows that the amount of CO_2 given off each cycle falls in a sequential fashion, figure 4b, main figure). The temperature cycling alone, is not responsible for this decay, as a sample cycled in argon for the same period sees no decay in CO_2 emission, (see supplementary information section S9). After the full 23 cycles, the amount of CO desorbed per cycle has reduced by 92% when cycling to 300 °C (90% in the case of cycling to only 200 °C, see supplementary information section S9). The amounts of carbon removed as carbon dioxide correspond to 505 $\mu mol_{carbon}\ g_{Fe\text{-}N/C}^{-1}$ for the sample cycled to 300 °C, which is equivalent to 6 $mg_{carbon}\ g_{Fe\text{-}N/C}^{-1}$ and leads to a 15% increase of total

surface area to 570 m^2 $g_{Fe\text{-}N/C}^{-1}$, and similarly a 13% increase in the micropore volume (see S10 for further details). The decay in CO_2 emission almost exactly matches an inverse square root law (line drawn on inset in figure 4b), which might be indicative of a diffusion process.

Despite the low amount of carbon removed, when these samples were tested for electrochemical activity, they showed a -28 mV shift of the ORR at 0.8 V or a 55% loss of kinetic current (59% at 0.85 V). In contrast, the sample cycled with argon instead of oxygen showed only a -3 mV shift. This indicates that loss of carbon is important in determining the activity of the sample (figure 4c, see supplementary information section S11 for plot of kinetic current density). TPD experiments utilising NO on the samples after oxygen cycling show that the high temperature peak of NO had decreased in area by 63% for the sample cycled at 200 °C and 71% for the sample cycled at 300 °C, suggesting that the cycling also removes the sites the NO binds to (figure 4d). The low temperature peak is largely unchanged, showing a 27% decrease in total area, although with a broadly similar peak height suggesting that it is caused by NO binding to different sites unaffected by the oxygen cycling.

There are two possible explanations for this behaviour – either active sites are being permanently removed by the thermal cycling, or each time the bare sample is exposed to oxygen, some of the oxygen binds to the sample in a form which is not removed by heating to 200 or 300 °C. In order to test the latter, after the final oxygen cycle the sample was treated at 600 °C in argon. Heat treatment at this temperature has recently been seen as being important during CO chemisorption experiments[27]. In our results, during this heat treatment, there is clear evidence of increased emission of CO_2 and in particular CO in the region above the cycling temperature (see supplementary information section S9). This region begins to see the decomposition of more stable oxygen groups such as carbonyls[50]. This high temperature treatment results in a 13 mV recovery of the electrochemical performance, equivalent to an 48% improvement in the kinetic current at 0.8V (34% at 0.85 V, see supplementary information section S11). The 600°C Ar-treated catalyst also sees a 90% recovery in the amount of oxygen chemisorption and subsequent CO_2 emission during the TPD process.

These results show that when Fe-N/C is exposed to oxygen, there are a limited number of sites where oxygen can bind and a small chance of binding as a more stable group which is less easily removed. When the oxygen groups are removed, most sites are regenerated allowing the binding of more oxygen despite the loss of carbon. These then bind oxygen in similar ratios of high to low stability groups. The decrease in availability of sites is reminiscent of a diffusion process on the basis of the decay in available sites (Inset, figure 4b). If the lower stability groups are consistently removed, over time higher stability groups build up. The build-up of these groups correlates with both lower electrochemical activity and lower NO sorption capacity, perhaps implying that the less stable groups are involved in both the electrochemistry and the binding of NO.

3.4. **Catalyst reactivation through thermal treatment and electrochemical reduction**

So far, we have shown that both NO and O_2 adsorption on the carbon surface can cause deactivation of the catalyst. In the case of NO, there is a discrepancy between the amount of NO adsorbed from the gas phase (131 $\mu mol_{NO}\ g_{Fe\text{-}N/C}^{-1}$ on the high temperature peak for catalyst heat treated at 600°C), and the amount determined electrochemically in our previous work (12 $\mu mol_{NO}\ g_{Fe\text{-}N/C}^{-1}$)[3]. Hence the reason for relevance of the result obtaining by the non-heat treated Fe-N/C sample in figure 2a, which achieves a value of 15 $\mu mol_{NO}\ g_{Fe\text{-}N/C}^{-1}$, much closer to the value from electrochemical stripping. Only by removing the adsorbates by pre-treatment at 600 °C can the sites be recovered and probed by gas phase NO measurements. In this case, it appears that the surface is blocked in the same way as seen for CO cryoadsorption[27]. The activation energy for the desorption of the NO in the high temperature

peak of the non 600°C treated sample, calculated in the same way as described above, is only slightly higher, at 64.1 kJ mol^{-1}, and is still second order, indicating that the mode of binding is similar to the sample heat treated to 600 °C before NO adsorption. These results caused us to wonder whether the as-prepared material is already partially poisoned by strongly bound O_2 species and water, and whether thermal treatment might be important in freeing the surface of strongly adsorbed oxygen species. In order to provide the most appropriate comparison for the poisoned samples, we took a sample of Fe-N/C catalyst which had been stored for one year under laboratory conditions (i.e. exposed to air, 22±4 °C), made an ink and tested it on an RDE, figure 5a.

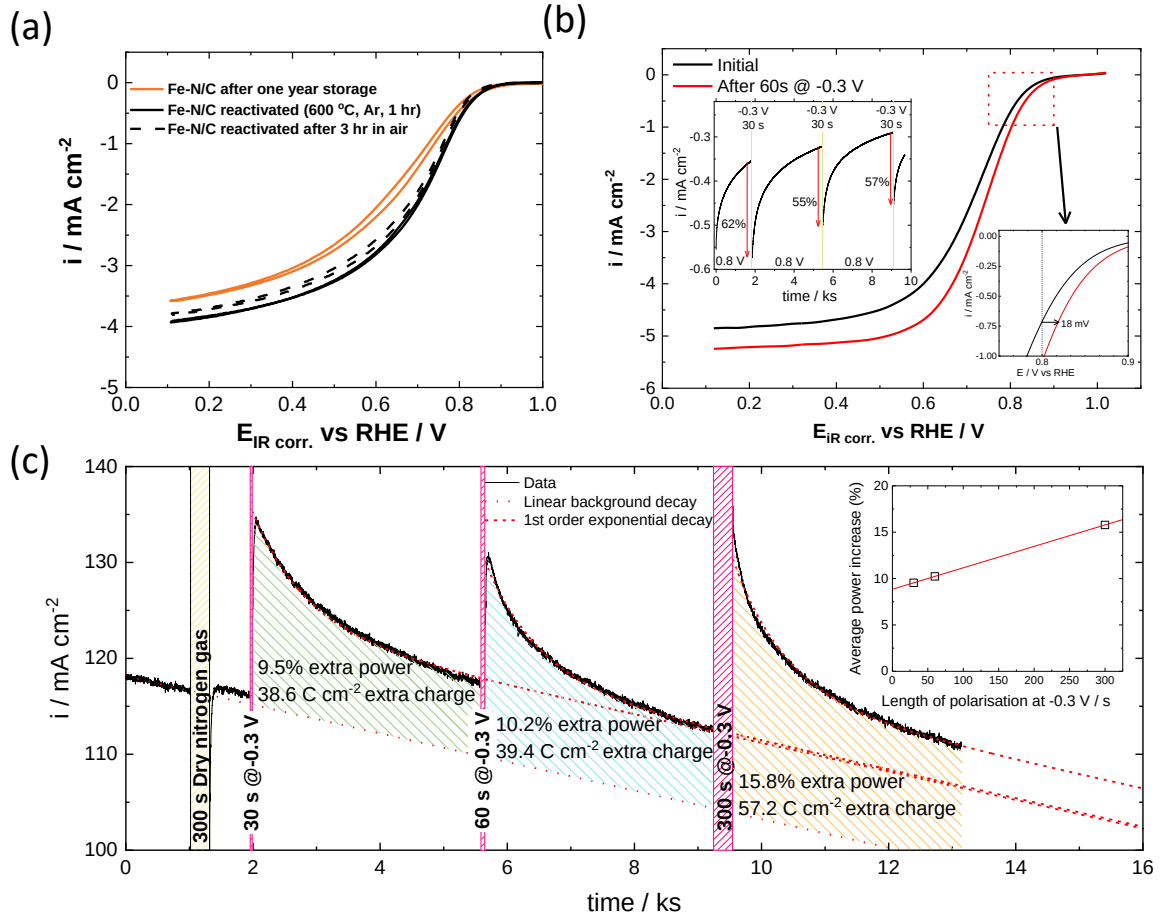

Figure 5 ¦ Recovery of catalyst performance by heat treatment and *operando* reductive treatment. RDE and Fuel Cell results. (a) ORR RDE measurements of Fe-N/C catalyst stored at room temperature for six months, reactivation in Ar at 600 °C, and after keeping at room temperature for 3 h before measurement. (b) ORR RDE measurements of Fe-N/C catalyst before and after being subjected to a reductive electrochemical treatment at -0.3 V vs RHE. Inset: ORR RDE chronamperometry at 0.8 V vs. RHE showing repeated reactivation at -0.3 V vs RHE. RDE results performed in O_2 saturated 0.5 M H_2SO_4, 1600 rpm, 5 mV s^{-1}, loading: 0.26 $mg_{Fe\text{-}N/C}$ cm^{-2}. (c) Single cell fuel cell activity of Fe-N/C catalyst operating at a cell voltage of 0.6 V after repeated reactivation at -0.3 V vs RHE. Loading of Fe-N/C catalyst 4 $mg_{Fe\text{-}N/C}$ cm^{-2} Results performed at 80°C cell temperature, 100% RH at both anode and cathode feed, except when dry nitrogen was used as indicated.

We also took a sample of that same catalyst and heat treated it at 600 °C in Ar for one hour, cooled it under argon and produced an electrode and tested it, as rapidly as possible, in order to minimise the potential for the sample to react with oxygen from the air. We found that the activity significantly improved from 0.65 mA cm^{-2} @0.8 V vs RHE to 1 mA cm^{-2} @0.8 V vs RHE, clearly showing that oxygen species adsorbed on the carbon are detrimental to the activity of the sample. A second identical electrode made of the reactivated catalyst was left for three hours in air and retested, and a slight drop in activity was observed, figure 4(a). This activation effect is relatively short-lived, with activity

levels slowly returning to normal after exposure to ambient air, showing that the deactivating oxygen species are formed rapidly simply by exposure to air, without any effects from operating in an acidic fuel cell environment.

Previously Malko et al have shown that strongly adsorbed NO can be electrochemically reductively stripped from the Fe-N/C leading to recovery from poisoning of the ORR[3]. We wondered whether the deleterious oxygen groups can also be reductively removed, potentially improving catalyst activity. Indeed, reductive treatment has been suggested by others as a way to improve performance[19]. When the catalyst is polarised at -0.3 V for 30 s in an RDE, the current increases by 62% at 0.8 V or equivalently there is a positive shift of 18 mV (figure 5b). The current then returns back to its original value over the next hour. The effect can be repeated multiple times, showing an improvement in ORR activity of ~55%.

We were intrigued to see whether the effect would carry over into fuel cell performance, and indeed it does, figure 5(c). In this diagram we show the performance of an operating fuel cell polarised at a potential of 0.6 V (for a fuel cell IV curve before these measurements, please see section S12). Initial operation of the fuel cell over a period of 30 minutes showed a slow pseudo-linear decay in performance of about 1.5 $\mu A\ cm^{-2}\ s^{-1}$. Polarisation of the fuel cells for 60 s at -0.3 V increases the current density at 0.6 V from 116 mA cm^{-2} to 134 mA cm^{-2} (figure 5c). The electrochemical stripping of the oxygen groups is rapid and significant – the improvement in activity is only marginally improved if the period at -0.3 V is extended from 30 s to 300 s suggesting most of the benefit occurs in the first few seconds of polarisation (figure 5c).

After the cathodic polarisation, the response of the fuel cell relaxes back to the pseudo linear decay which we previously saw, however that linear decay is at a higher level than before the cathodic treatment. Fitting of these decays to a first-order exponential decay gave a good fit with a common time constant for all three transients of 840 s (for details of the fitting procedure, see supplementary information section S13). We analysed the average increase in current density associated with the negative polarisation of the fuel cell and find that there is an increase of average current density (and thus power output) of 10-15%, and that the effect shows a linear increase with the length of cathodic polarisation, figure 5c (inset).

Previous studies have hypothesised that a water flooding effect may be responsible for poor performance in these cathode materials. To test whether the period at -0.3 V was simply removing water from the pores, we replaced the period at -0.3 V with a period of 5 mins where the cathode is flushed with dry nitrogen at open circuit potential. The cell showed little signs of improvement after this, indicating that removal of water is not the cause of the improvement. It is intriguing that there is a slow degradation of performance which appears unaffected by the reductive transients. This very slow degradation might be associated with physical loss of iron from the active sites. We can characterise the effect of the reductive transients not only in terms of the extra power produced but also by the increased lifetime of the cell. This extra lifetime comes about because the reductive transient leads to a linear decay which is at a higher level than before the transient, and thus an increased lifespan of the cell before it reaches any cutoff voltage. We find that for the 30 s reductive transient, we increase the cell lifetime by 5300 s (see supplementary information section S13 for details). This is an interesting aspect of the reductive treatment – that it not only increases the power output of the cell for a transient period, but also effectively increases the lifespan of the fuel cell system.

3.5. Comparison of Fe-NC interaction with NO and O_2 in gas phase and liquid phase environments

In order to summarise the results in this paper, the cartoon in figure 6 compares the effect of the two different gaseous species we have studied (NO (left) and O_2 (right)), and the two different environments (gas phase in the absence of water (upper half) and solution phase in the presence of water containing electrolyte (lower half)) as a function of catalyst pre-treatment (aged in air at room temperature, or treated at 600 °C under argon). The centre of this figure, figure 6(a) shows the effect of aging and heat-treatment of the catalyst.

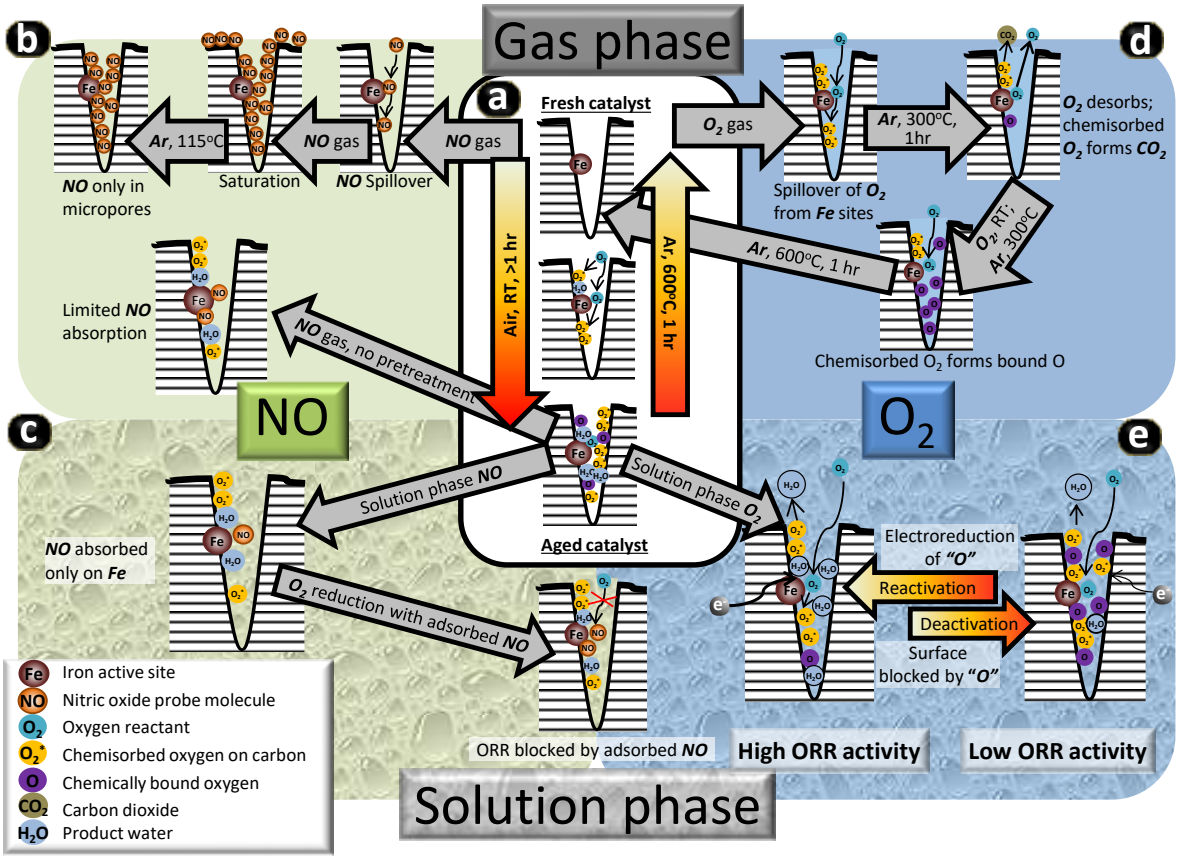

Figure 6 ¦ Cartoon of Fe-N/C interaction with O_2 and NO in the *gas* and *solution* phases (a) aging of catalyst after heat treatment at 600°C and exposure to the atmosphere. (b) *Gas phase* NO chemisorption and how it is affected by the state of the catalyst and heat treatment. (c) *Solution phase* NO adsorption associated with aged/O_2 exposed Fe-N/C catalysts; (d) *Gas phase* O_2 chemisorption and how the surface state of the Fe-N/C is affected by O chemisorption and reaction; (e) *Solution phase* O_2 reaction including electrochemical reactivation.

When the catalyst is initially produced, or after it has been treated under argon at 600 °C, the micropore in which the iron sites are present are free of adsorbates, and the iron sites are unaffected by any coordinated species (top). On cooling and exposure to air, water starts to adsorb within the micropores, and oxygen coordinates with the iron and then proceeds to spillover onto the surface forming chemisorbed oxygen species and further reacting to form carbon species such as epoxides. These reactions are probably assisted by the formation of free radical sites at the carbon surface by the heat treatment process[51] which then either directly react with oxygen or react with the spillover oxygen coming from the iron site.

Over longer periods on storage in air, more water adsorbs in the micropores, and the chemically bound oxygen species convert into more intractable species such as aldehydes. This process deactivates the catalyst through two different mechanisms. First, it decreases the available sites surrounding the catalyst available to accept spillover oxygen (e.g. consider the decay in oxygen adsorption with

number of cycles of oxygen exposure – inset in figure 4b); and secondly as has been found in literature, modification of the carbon surface modifies the local electronic environment of the iron via local shifts in the Fermi level[19].

The gas phase adsorption of NO in the absence of water, figure 6(b), involves the adsorption of NO on the Fe sites and subsequent spillover onto the surface of the micropore and beyond. Heating the sample for one hour under argon desorbs the NO not in micropores. In contrast, if the sample is treated with gas phase NO without preheating the sample to 600 ^{o}C in argon, then the adsorbed water and strongly bound oxygen drastically reduce the amount of NO adsorbed, giving similar amounts to that found in solution phase adsorption, figure 6(c). During solution phase adsorption of NO, those NO blocked sites lead to a reduction in ORR activity which is measured and related to the catalyst turnover number.

Gas phase oxygen sorption, figure 6(d), is in many ways similar to NO sorption, relying in part on a spillover mechanism associated with the oxygen adsorbing on the Fe. However, in this case, instead of desorbing as O_2, > 99% of the oxygen desorbs as CO_2 suggesting that the majority of the oxygen is bound to the carbon in the form of relatively easily decomposed groups such as epoxides, although a small amount of oxygen goes on to form more intractable oxygen containing species such as aldehyde.

On repeated exposure to oxygen the amount of strongly adsorbed oxygen species grows on the surface, leading to an increasingly less active surface – only when the temperature is raised to 600 ^{o}C is this intractable oxygen removed from the surface to regenerate the adsorbate free surface. During ORR testing in the solution phase, deactivation of the catalyst follows a similar process to that seen in the gas phase apart from the additional effect of water. Over long-term polarisation of the electrode during oxygen reduction, there is a build-up of intractable oxygen species on the surface, and a majority of these can be removed by applying a strong reducing electrochemical polarisation.

4. Conclusions

On the basis of NO chemisorption results it appears as if in acid the active site for oxygen reduction in Fe-N/C catalysts is associated with the micropores of that material. We have shown that the surface of Fe-N/C catalysts are strongly affected by adventitious adsorbates which modulate and modify the performance of those catalysts towards the oxygen reduction reaction in liquid (RDE) and solid (fuel cell) electrolytes. Those adsorbed species comprise water and oxygen containing species, which range from chemisorbed oxygen to oxygen incorporated in the carbon structure in weakly bound (e.g. epoxide) and strongly bound (e.g. aldehydic) forms. Both water and the oxygen species are formed on storage of the catalysts in air at room temperature. The performance of the Fe-N/C catalyst is negatively affected by the presence of these adsorbates, either through site blocking on the carbon surface surrounding the Fe active site or due to modification of the local electronic structure and shift of the Fermi level. Treatment of the surface to remove those adsorbed species utilising either thermal treatment (heating at 600^{o}C under argon), or electrochemical reduction (-0.3 V vs. RHE) leads to activation of the catalyst due to removal of the oxygenated species. During the heat treatment process, it has been shown that chemisorbed oxygen is mainly removed as CO_2, strengthening the argument that the oxygen is incorporated into the carbon surrounding the Fe active site. Electrochemical reduction of the oxygen containing species leads to activation of the surface, and there is a relaxation of the current back towards a baseline performance with a time constant of 800-900 s. The ability to compare electrochemical surface activity measurements on Fe-N/C catalysts to results obtained on the same catalysts using gas phase chemisorption is complicated by the presence of water and the aforementioned adsorbates which form during the necessary exposure of these catalysts to electrolyte and oxygen. As a result, gas-phase chemisorption experiments overestimate

the number of available sites, as under the usual operating environments containing water and oxygen, many of the sites are unavailable for reaction. The NO adsorption process under water and oxygen free conditions appears to be associated with NO adsorption on the Fe sites followed by spillover onto the surface of the micropores.

5. Acknowledgements

The research leading to these results has received funding from the UK Engineering and Physical Sciences Research Council under projects EP/R023581/1 and EP/P024807/1, and the Fuel Cells and Hydrogen 2 Joint Undertaking under grant agreement No 779366, CRESCENDO. This Joint Undertaking receives support from the European Union's Horizon 2020 research and innovation programme, Hydrogen Europe and Hydrogen Europe Research.

6. Data availability

The data presented in the figures of this paper are available to download at DOI: (DOI inserted at proofing stage].

7. References

[1] N.M. Markovic, Interfacing electrochemistry, Nature Materials, 12 (2013) 101. 10.1038/nmat3554.
[2] M.K. Debe, Electrocatalyst approaches and challenges for automotive fuel cells, Nature, 486 (2012) 43-51. 10.1038/nature11115.
[3] D. Malko, A. Kucernak, T. Lopes, In situ electrochemical quantification of active sites in Fe–N/C non-precious metal catalysts, Nature Communications, 7 (2016) 13285. http://dx.doi.org/10.1038/ncomms13285.
[4] M. Lefèvre, E. Proietti, F. Jaouen, J.-P. Dodelet, Iron-Based Catalysts with Improved Oxygen Reduction Activity in Polymer Electrolyte Fuel Cells, Science, 324 (2009) 71. 10.1126/science.1170051.
[5] E. Proietti, F. Jaouen, M. Lefèvre, N. Larouche, J. Tian, J. Herranz, J.-P. Dodelet, Iron-based cathode catalyst with enhanced power density in polymer electrolyte membrane fuel cells, Nature Communications, 2 (2011) 416. 10.1038/ncomms1427.
[6] G. Wu, K.L. More, C.M. Johnston, P. Zelenay, High-Performance Electrocatalysts for Oxygen Reduction Derived from Polyaniline, Iron, and Cobalt, Science, 332 (2011) 443. 10.1126/science.1200832.
[7] A. Zitolo, V. Goellner, V. Armel, M.-T. Sougrati, T. Mineva, L. Stievano, E. Fonda, F. Jaouen, Identification of catalytic sites for oxygen reduction in iron- and nitrogen-doped graphene materials, Nature Materials, 14 (2015) 937. 10.1038/nmat4367

https://www.nature.com/articles/nmat4367#supplementary-information.
[8] U.I. Kramm, J. Herranz, N. Larouche, T.M. Arruda, M. Lefèvre, F. Jaouen, P. Bogdanoff, S. Fiechter, I. Abs-Wurmbach, S. Mukerjee, J.-P. Dodelet, Structure of the catalytic sites in Fe/N/C-catalysts for O2-reduction in PEM fuel cells, Physical Chemistry Chemical Physics, 14 (2012) 11673-11688. 10.1039/C2CP41957B.
[9] I. Martinaiou, A. Videla, N. Weidler, M. Kubler, W.D.Z. Wallace, S. Paul, S. Wagner, A. Shahraei, R.W. Stark, S. Specchia, U.I. Kramm, Activity and degradation study of an Fe-N-C catalyst for ORR in Direct Methanol Fuel Cell (DMFC), Applied Catalysis B-Environmental, 262 (2020). 10.1016/j.apcatb.2019.118217.
[10] G. Liu, X.G. Li, P. Ganesan, B.N. Popov, Development of non-precious metal oxygen-reduction catalysts for PEM fuel cells based on N-doped ordered porous carbon, Applied Catalysis B-Environmental, 93 (2009) 156-165. 10.1016/j.apcatb.2009.09.025.

[11] D. Malko, Y. Guo, P. Jones, G. Britovsek, A. Kucernak, Heterogeneous iron containing carbon catalyst (Fe-N/C) for epoxidation with molecular oxygen, Journal of Catalysis, 370 (2019) 357-363. https://doi.org/10.1016/j.jcat.2019.01.008.
[12] R.V. Jagadeesh, H. Junge, M. Beller, "Nanorust"-catalyzed Benign Oxidation of Amines for Selective Synthesis of Nitriles, ChemSusChem, 8 (2015) 92-96. 10.1002/cssc.201402613.
[13] X. Cui, Y. Li, S. Bachmann, M. Scalone, A.-E. Surkus, K. Junge, C. Topf, M. Beller, Synthesis and Characterization of Iron–Nitrogen-Doped Graphene/Core–Shell Catalysts: Efficient Oxidative Dehydrogenation of N-Heterocycles, Journal of the American Chemical Society, 137 (2015) 10652-10658. 10.1021/jacs.5b05674.
[14] W. Liu, L. Zhang, X. Liu, X. Liu, X. Yang, S. Miao, W. Wang, A. Wang, T. Zhang, Discriminating Catalytically Active FeNx Species of Atomically Dispersed Fe–N–C Catalyst for Selective Oxidation of the C–H Bond, Journal of the American Chemical Society, 139 (2017) 10790-10798. 10.1021/jacs.7b05130.
[15] H.A. Gasteiger, S.S. Kocha, B. Sompalli, F.T. Wagner, Activity benchmarks and requirements for Pt, Pt-alloy, and non-Pt oxygen reduction catalysts for PEMFCs, Applied Catalysis B: Environmental, 56 (2005) 9-35. https://doi.org/10.1016/j.apcatb.2004.06.021.
[16] N. Ramaswamy, U. Tylus, Q. Jia, S. Mukerjee, Activity Descriptor Identification for Oxygen Reduction on Nonprecious Electrocatalysts: Linking Surface Science to Coordination Chemistry, Journal of the American Chemical Society, 135 (2013) 15443–15449. 10.1021/ja405149m.
[17] N.R. Sahraie, U.I. Kramm, J. Steinberg, Y. Zhang, A. Thomas, T. Reier, J.-P. Paraknowitsch, P. Strasser, Quantifying the density and utilization of active sites in non-precious metal oxygen electroreduction catalysts, Nature Communications, 6 (2015) 8618. 10.1038/ncomms9618

https://www.nature.com/articles/ncomms9618#supplementary-information.
[18] M. Ferrandon, A.J. Kropf, D.J. Myers, K. Artyushkova, U. Kramm, P. Bogdanoff, G. Wu, C.M. Johnston, P. Zelenay, Multitechnique Characterization of a Polyaniline–Iron–Carbon Oxygen Reduction Catalyst, The Journal of Physical Chemistry C, 116 (2012) 16001-16013. 10.1021/jp302396g.
[19] C.H. Choi, H.-K. Lim, M.W. Chung, G. Chon, N. Ranjbar Sahraie, A. Altin, M.-T. Sougrati, L. Stievano, H.S. Oh, E.S. Park, F. Luo, P. Strasser, G. Dražić, K.J.J. Mayrhofer, H. Kim, F. Jaouen, The Achilles' heel of iron-based catalysts during oxygen reduction in an acidic medium, Energy & Environmental Science, 11 (2018) 3176-3182. 10.1039/C8EE01855C.
[20] J.L. Kneebone, S.L. Daifuku, J.A. Kehl, G. Wu, H.T. Chung, M.Y. Hu, E.E. Alp, K.L. More, P. Zelenay, E.F. Holby, M.L. Neidig, A Combined Probe-Molecule, Mössbauer, Nuclear Resonance Vibrational Spectroscopy, and Density Functional Theory Approach for Evaluation of Potential Iron Active Sites in an Oxygen Reduction Reaction Catalyst, The Journal of Physical Chemistry C, 121 (2017) 16283-16290. 10.1021/acs.jpcc.7b03779.
[21] D. Malko, A. Kucernak, Kinetic isotope effect in the oxygen reduction reaction (ORR) over Fe-N/C catalysts under acidic and alkaline conditions, Electrochem. Commun., 83 (2017) 67-71. http://dx.doi.org/10.1016/j.elecom.2017.09.004.
[22] D. Malko, T. Lopes, E.A. Ticianelli, A. Kucernak, A catalyst layer optimisation approach using electrochemical impedance spectroscopy for PEM fuel cells operated with pyrolysed transition metal-N-C catalysts, Journal of Power Sources, 323 (2016) 189-200. http://dx.doi.org/10.1016/j.jpowsour.2016.05.035.
[23] D. Malko, T. Lopes, E. Symianakis, A.R. Kucernak, The intriguing poison tolerance of non-precious metal oxygen reduction reaction (ORR) catalysts, Journal of Materials Chemistry A, 4 (2016) 142-152. http://dx.doi.org/10.1039/c5ta05794a.
[24] D. Malko, A. Kucernak, T. Lopes, Performance of Fe–N/C Oxygen Reduction Electrocatalysts toward NO2–, NO, and NH2OH Electroreduction: From Fundamental Insights into the Active Center to a New Method for Environmental Nitrite Destruction, Journal of the American Chemical Society, 138 (2016) 16056-16068. http://dx.doi.org/10.1021/jacs.6b09622.

[25] T. Lopes, A. Kucernak, D. Malko, E.A. Ticianelli, Mechanistic Insights into the Oxygen Reduction Reaction on Metal–N–C Electrocatalysts under Fuel Cell Conditions, ChemElectroChem, 3 (2016) 1580-1590. http://dx.doi.org/10.1002/celc.201600354.
[26] M. Primbs, Y. Sun, A. Roy, D. Malko, A. Mehmood, M.-T. Sougrati, P.-Y. Blanchard, G. Granozzi, T. Kosmala, G. Daniel, P. Atanassov, J. Sharman, C. Durante, A. Kucernak, D. Jones, F. Jaouen, P. Strasser, Establishing reactivity descriptors for platinum group metal (PGM)-free Fe–N–C catalysts for PEM fuel cells, Energy & Environmental Science, 13 (2020) 2480-2500. 10.1039/D0EE01013H.
[27] F. Luo, C.H. Choi, M.J.M. Primbs, W. Ju, S. Li, N.D. Leonard, A. Thomas, F. Jaouen, P. Strasser, Accurate Evaluation of Active-Site Density (SD) and Turnover Frequency (TOF) of PGM-Free Metal–Nitrogen-Doped Carbon (MNC) Electrocatalysts using CO Cryo Adsorption, ACS Catalysis, 9 (2019) 4841-4852. 10.1021/acscatal.9b00588.
[28] V.C.A. Ficca, C. Santoro, A. D'Epifanio, S. Licoccia, A. Serov, P. Atanassov, B. Mecheri, Effect of Active Site Poisoning on Iron−Nitrogen−Carbon Platinum-Group-Metal-Free Oxygen Reduction Reaction Catalysts Operating in Neutral Media: A Rotating Disk Electrode Study, ChemElectroChem, 7 (2020) 3044-3055. https://doi.org/10.1002/celc.202000754.
[29] D. Holmes Parker, M.E. Jones, B.E. Koel, Determination of the reaction order and activation energy for desorption kinetics using TPD spectra: Application to D2 desorption from Ag(111), Surface Science, 233 (1990) 65-73. https://doi.org/10.1016/0039-6028(90)90176-9.
[30] T.Q. Nguyen, M.C.S. Escaño, H. Kasai, Nitric Oxide Adsorption Effects on Metal Phthalocyanines, The Journal of Physical Chemistry B, 114 (2010) 10017-10021. 10.1021/jp1035426.
[31] C. Rovira, K. Kunc, J. Hutter, P. Ballone, M. Parrinello, A comparative study of O2, CO, and NO binding to iron–porphyrin, International Journal of Quantum Chemistry, 69 (1998) 31-35. 10.1002/(SICI)1097-461X(1998)69:1<31::AID-QUA5>3.0.CO;2-Y.
[32] T.Q. Nguyen, M.C.S. Escaño, N. Shimoji, H. Nakanishi, H. Kasai, Adsorption of diatomic molecules on iron tape-porphyrin: A comparative study, Physical Review B, 77 (2008) 195307. 10.1103/PhysRevB.77.195307.
[33] E. Ashori, F. Nazari, F. Illas, Influence of NO and (NO)2 adsorption on the properties of Fe-N4 porphyrin-like graphene sheets, Physical Chemistry Chemical Physics, 19 (2017) 3201-3213. 10.1039/C6CP07898B.
[34] H. Teng, E.M. Suuberg, Chemisorption of nitric oxide on char. 1. Reversible nitric oxide sorption, The Journal of Physical Chemistry, 97 (1993) 478-483. 10.1021/j100104a033.
[35] K. Kaneko, N. Fukuzaki, K. Kakei, T. Suzuki, S. Ozeki, Enhancement of nitric oxide dimerization by micropore fields of activated carbon fibers, Langmuir, 5 (1989) 960-965. 10.1021/la00088a014.
[36] S. Matzner, H.P. Boehm, Influence of nitrogen doping on the adsorption and reduction of nitric oxide by activated carbons, Carbon, 36 (1998) 1697-1703. https://doi.org/10.1016/S0008-6223(98)90047-1.
[37] K. Kaneko, Z. Wang, T. Suzuki, S. Ozeki, N. Kosugi, H. Kuroda, Micropore filling of supercritical NO on Cu-doped iron oxide dispersed activated carbon fibers, Journal of Colloid and Interface Science, 142 (1991) 489-496. https://doi.org/10.1016/0021-9797(91)90078-M.
[38] K. Kaneko, T. Ohta, S. Ozeki, N. Kosugi, H. Kuroda, Chemisorption-assisted micropore filling of no on Cu, Ni, and Co oxide-dispersed activated carbon fibers, Applied Surface Science, 33-34 (1988) 355-363. https://doi.org/10.1016/0169-4332(88)90327-3.
[39] B. Xia, J. Phillips, C.-K. Chen, L.R. Radovic, I.F. Silva, J.A. Menéndez, Impact of Pretreatments on the Selectivity of Carbon for NOx Adsorption/Reduction, Energy & Fuels, 13 (1999) 903-906. 10.1021/ef9802680.
[40] J. Alcañiz-Monge, A. Bueno-López, M.Á. Lillo-Rodenas, M.J. Illán-Gómez, NO adsorption on activated carbon fibers from iron-containing pitch, Microporous and Mesoporous Materials, 108 (2008) 294-302. https://doi.org/10.1016/j.micromeso.2007.04.011.
[41] K. Kaneko, Anomalous micropore filling of nitric oxide on .alpha.-iron hydroxide oxide-dispersed activated carbon fibers, Langmuir, 3 (1987) 357-363. 10.1021/la00075a014.

[42] R.N. Smith, D. Lesnini, J. Mooi, The Anomalous Adsorptive Properties of Nitric Oxide, The Journal of Physical Chemistry, 60 (1956) 1063-1066. 10.1021/j150542a011.
[43] L.J. Zhong, C. Frandsen, S. Morup, Y. Hu, C. Pan, L.N. Cleemann, J.O. Jensen, Q.F. Li, Fe-57-Mossbauer spectroscopy and electrochemical activities of graphitic layer encapsulated iron electrocatalysts for the oxygen reduction reaction, Applied Catalysis B-Environmental, 221 (2018) 406-412. 10.1016/j.apcatb.2017.09.014.
[44] J.L. Hueso, J.P. Espinós, A. Caballero, J. Cotrino, A.R. González-Elipe, XPS investigation of the reaction of carbon with NO, O2, N2 and H2O plasmas, Carbon, 45 (2007) 89-96. https://doi.org/10.1016/j.carbon.2006.07.021.
[45] M. Dubey, S.L. Bernasek, J. Schwartz, Highly Sensitive Nitric Oxide Detection Using X-ray Photoelectron Spectroscopy, Journal of the American Chemical Society, 129 (2007) 6980-6981. 10.1021/ja070943x.
[46] H.S. Jeong, C.M. Kim, Reaction of NO on vanadium oxide surfaces: Observation of the NO dimer formation, BULLETIN-KOREAN CHEMICAL SOCIETY, 28 (2007) 413.
[47] Z. Shuxian, W.K. Hall, G. Ertl, H. Knözinger, X-ray photoemission study of oxygen and nitric oxide adsorption on MoS2, Journal of Catalysis, 100 (1986) 167-175.
[48] K. Kaneko, K. Murata, An analytical method of micropore filling of a supercritical gas, Adsorption, 3 (1997) 197-208. 10.1007/bf01650131.
[49] A. Lipatov, M.J.F. Guinel, D.S. Muratov, V.O. Vanyushin, P.M. Wilson, A. Kolmakov, A. Sinitskii, Low-temperature thermal reduction of graphene oxide: In situ correlative structural, thermal desorption, and electrical transport measurements, Applied Physics Letters, 112 (2018) 053103. 10.1063/1.4996337.
[50] M. Acik, G. Lee, C. Mattevi, A. Pirkle, R.M. Wallace, M. Chhowalla, K. Cho, Y. Chabal, The Role of Oxygen during Thermal Reduction of Graphene Oxide Studied by Infrared Absorption Spectroscopy, The Journal of Physical Chemistry C, 115 (2011) 19761-19781. 10.1021/jp2052618.
[51] U. Green, K. Keinan-Adamsky, S. Attia, Z. Aizenshtat, G. Goobes, S. Ruthstein, H. Cohen, Elucidating the role of stable carbon radicals in the low temperature oxidation of coals by coupled EPR-NMR spectroscopy - a method to characterize surfaces of porous carbon materials, Physical Chemistry Chemical Physics, 16 (2014) 9364-9370. 10.1039/c4cp00791c.